JACS Au
AN OPEN ACCESS JOURNAL OF THE AMERICAN CHEMICAL SOCIETY

pubs.acs.org/jacsau
Article

Thick ZnS Shells on $CsPbBr_3$ Quantum Dots by Colloidal-Atomic Layer Deposition for Enhanced Photoluminescence and Stability

Justice A. Teku, Derrick A. Taylor, and Jong-Soo Lee*

Cite This: JACS Au 2025, 5, 4036−4043
Read Online

ACCESS | Metrics & More | Article Recommendations | Supporting Information

ABSTRACT: The colloidal-atomic layer deposition (c-ALD) method is employed to grow a zinc sulfide (ZnS) shell on $CsPbBr_3$ perovskite quantum dots (PeQDs) to form $CsPbBr_3$/ZnS core/shell heterostructures to address the intrinsic stability challenges of PeQDs. The c-ALD process offers layer by layer control over the thickness of the shell, enabling uniform and conformal encapsulation, which significantly passivates the surface defects and enhances the optical properties of the PeQDs. This approach significantly improves photoluminescence quantum yield, increases environmental stability, and prolongs the average radiative lifetime of the $CsPbBr_3$ PeQDs. The structural and spectroscopic analysis confirms the formation of a thick and uniform ZnS shell. Furthermore, the resulting core/shell PeQDs exhibit exceptional thermal, photostability, and aqueous durability, surpassing the limitations of pristine $CsPbBr_3$ PeQDs. This work opens new opportunities for the c-ALD method to be integrated into perovskite core/shell heterostructures for advancing optoelectronic technologies.

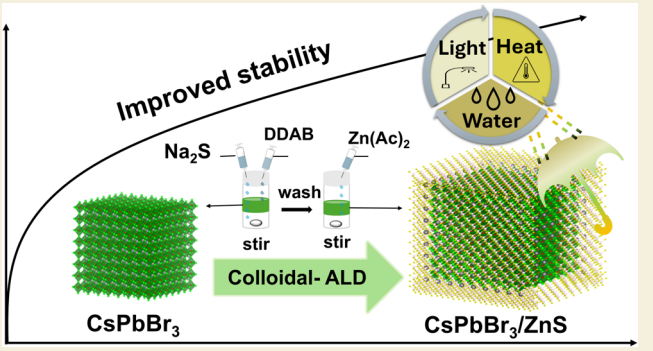

KEYWORDS: *zinc sulfide, c-ALD, heterostructure, core/shell, stability, perovskite*

INTRODUCTION

Colloidal cesium lead halide perovskite quantum dots (PeQDs) have received significant attention as a multipurpose material. They exhibit near-unity photoluminescence quantum yield, narrow emission line width, wide color gamut, and high defect tolerance.[1−5] Their excellent optical properties have encouraged its application in photovoltaics,[6−8] light-emitting diodes (LEDs),[9−14] lasers,[15,16] and photodetectors.[17−19] Despite their excellent optical properties, the PeQDs exhibited poor environmental stability and surface defects during processing and storage, so therefore, recent researchers have introduced a perovskite core/shell heterostructure to solve the stability and defect challenges. The core/shell heterostructure optimizes the ionic surface nature of the PeQDs by creating a physical blockage that protects them from extrinsic factors,[20−23] cut off the ion migration channel, and increase photoluminescence stability.[24−26] The perovskite core/shell heterostructure significantly differs from the conventional method due to their soft ionic nature, high ion mobility, and rapid reaction rate.[26,27] The shell materials used in the perovskite core/shell heterostructure, including metal oxides,[28−34] other perovskite,[35−37] and metal chalcogenides[20,38−49] increase the luminescence and passivate surface defects of the PeQDs. However, despite these improvements, many of these materials offer only temporal stability with some having insulating properties that can hinder their usage in optoelectronic applications.

Among the various shell candidates, metal chalcogenide shells are prominent for their general ability to improve the overall stability and photoluminescence of the PeQDs. Zinc sulfide (ZnS), a wide band gap semiconductor material, is regarded as one of the essential shell candidates that effectively passivates, protects, and eliminates dangling bonds and surface defects on the surface of PeQDs. Numerous studies on perovskites have reported and validated the ZnS hypothesis. However, synthesizing ZnS shells requires high temperatures, which remains a significant challenge as it damages the soft ionic nature of the perovskite core. Nag and co-workers reported a pseudo type II $CsPbBr_3$/ZnS core/shell heterostructure synthesized at 120 °C after stabilizing $CsPbBr_3$ with oleylammonium bromide. Their resulting $CsPbBr_3$/ZnS core/shell improved photostability and prolonged the average lifetime of the PeQDs.[44] Similarly, Hong et al. synthesized an epitaxial ZnS shell on $CsPb(Br_{1-x}Cl_x)_3$ using the hot

Received: May 23, 2025
Revised: July 2, 2025
Accepted: July 24, 2025
Published: August 1, 2025

injection method at 140 °C, and their finding shows that the shell protected the perovskite nanocrystals from environmental factors and extended the LED operational lifetime.[47] Wang and co-worker further reported enhanced photostability and thermal stability in Zn-doped $CsPbBr_3$/ZnS heterostructure core/shell.[50] Although the core/shell heterostructure improves the optical properties of the perovskite, the resulting shell generally exhibits nonuniformity, with no clear evidence of facet-to-facet orientation. To avoid the high-temperature constraints and preserve the integrity of the perovskite to grow a uniform ZnS shell, a room-temperature synthesis approach, colloidal-atomic layer deposition (c-ALD), has been introduced.

c-ALD utilizes a self-limiting half-reaction process designed to deposit new inorganic materials at the surface of the colloidal core materials under controlled conditions.[51,52] The concept involves mixing the core nanocrystal capped with organic ligands in nonpolar solvents, with the shell precursors in polar solvents, triggering a biphasic reaction. This shelling technique provides exceptional colloidal stability to nanocrystals, providing resistance against extrinsic factors, polar solvents, and ligand dynamicity, hence overcoming the limitations of the high-temperature synthesis reported.[33,34,53−55] Pioneering work by Talapin's group demonstrated using c-ALD to grow CdS shells on CdSe nanostructures,[52] Bawendi's group has applied c-ALD for the sequential growth of true CdS shell on the PbS QDs, enabling fine control over the CdS shell thickness.[51] Loiudice et al. expanded the application of c-ALD by growing tunable metal oxide shells on various nanocrystals, including perovskite, metal oxides, and metals, while preserving their colloidal stability.[53−55] Green et al. further applied the c-ALD to grow a metal oxide shell on semiconductor nanocrystals creating organic/inorganic hybrid materials.[34] From the perspective of perovskite nanocrystals, alumina shells synthesized by c-ALD exhibited outstanding resistance to degradation in an inert atmosphere and significantly enhanced photoluminescence quantum yield.[33] However, most reported c-ALD shelling $CsPbBr_3$ perovskite nanocrystals have focused solely on forming metal oxides, with no reported or published work exploring metal chalcogenide shells on perovskite.

This work presents a c-ALD method to grow zinc sulfide (ZnS) on halide-rich $CsPbBr_3$ PeQDs at room temperature. The process involves sequential mixing of the anion precursor (S^{2-}) and the cation precursor (Zn^{2+}) with PeQDs solution, utilizing oleylamine and (di-n-dodecyl) dimethylammonium bromide (DDAB) as ligands and a phase transfer agent. The c-ALD process provides layer by layer control over the thickness of the shell, enabling uniform encapsulation and hence significantly passivates the surface defects and enhances the optical properties of the PeQDs. The structural and spectroscopic analyses confirmed the formation of a thick ZnS shell around the core $CsPbBr_3$ PeQDs. The resulting core/shell significantly improves the photoluminescence quantum yield, environmental stability, and radiative lifetime of the $CsPbBr_3$ PeQDs. The ZnS shell provides remarkable stability, with only 15% degradation after 48 h of continuous heat exposure and 20% after 648 h of continuous light exposure, compared to nearly 98% degradation observed in unprotected pristine $CsPbBr_3$ PeQDs. Additionally, the ZnS shell tremendously enhances the aqueous stability, maintaining structural integrity for 504 h in water, whereas the unprotected $CsPbBr_3$ PeQDs degrade within 12 h. This work highlights the potential of the c-ALD method for advancing perovskite core/shell heterostructures and paves the way for further improvements in optoelectronic technologies.

RESULTS AND DISCUSSION

The c-ALD $CsPbBr_3$/ZnS core/shell heterostructure is synthesized in two stages. The first stage involves the synthesis of halide-rich pristine $CsPbBr_3$ PeQDs[56,57] (see details in the experimental procedure). The purified pristine PeQDs were subjected to the second stage, whereby the c-ALD approach was used to grow the ZnS shell on the pristine PeQDs. This step is very delicate and can only be achieved by using halide-rich $CsPbBr_3$, the presence of DDAB, and a biphasic system. The biphasic system of c-ALD reaction proceeded through coupled interaction between the PeQDs solution (nonpolar) phase and reagents in the polar aqueous phase. The c-ALD biphasic reaction comprises two half reactions, whereby the separate half reactions involve transferring either the sulfur ion (S^{2-}) or zinc ion (Zn^{2+}) from their polar aqua phase to the nonpolar phase, enabling the formation of ZnS shell on the PeQDs. The half reactions are combined in the chemical reactions below.

Scheme 1 comprises two half reactions that combine to form a complete c-ALD process. The first half reaction proceeds via

Scheme 1. Chemical Reactions Illustrating ZnS Formation via c-ALD on the PeQDs

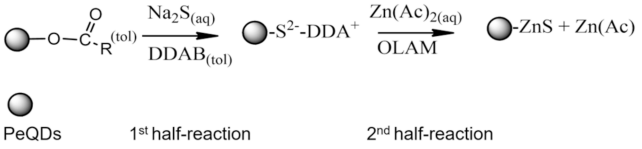

a ligand exchange process in a biphasic system, whereby the organic ligands on the PeQDs are replaced by sulfur ions with the help of a DDAB. DDAB facilitates the formation of an interfacial region between the polar and nonpolar solvents, hence promoting the migration of sulfur ions to the nonpolar solvent. The sulfur ion effectively displaces the native organic ligand and binds to the PeQDs as a ligand, while residual DDA ions stabilize the sulfur-capped PeQDs. Subsequently, the second half reaction was initiated by adding a Zn ion precursor in the presence of the primary amine. The Zn ions reacted with sulfur-capped PeQDs, forming a ZnS shell. The amine added acts as a transfer agent and surface ligand, hence stabilizing the ZnS-coated PeQDs. The c-ALD process was repeated, enabling thicker ZnS growth on the $CsPbBr_3$. The experimental procedure of the c-ALD process is illustrated in Scheme 2. Detailed procedure for the synthesis is in the Experimental Section.

Figure 1a shows a schematic illustration of the $CsPbBr_3$/ZnS core/shell heterostructure, where $CsPbBr_3$ core PQDs are uniformly encapsulated by a ZnS shell. The X-ray diffraction (XRD) patterns of the core/shell heterostructure PeQDs (Figure 1b) clearly reveal the presence of two distinct crystalline phases. Compared to the pristine $CsPbBr_3$ core, the $CsPbBr_3$/ZnS core/shell heterostructure exhibits additional peaks that match well with the standard diffraction pattern of ZnS, confirming successful shell formation. Transmission electron microscopy (TEM) images show the average size of the pristine $CsPbBr_3$ PeQDs with an average size 14.2 ± 1.4 nm (Figure S1a,d), which gradually increases to 15.3 ± 1.8

https://doi.org/10.1021/jacsau.5c00651
JACS Au 2025, 5, 4036−4043

Scheme 2. Illustrate the Scheme and Experimental Procedure of Forming ZnS Shell on $CsPbBr_3$ PeQDs Using c-ALD Processes

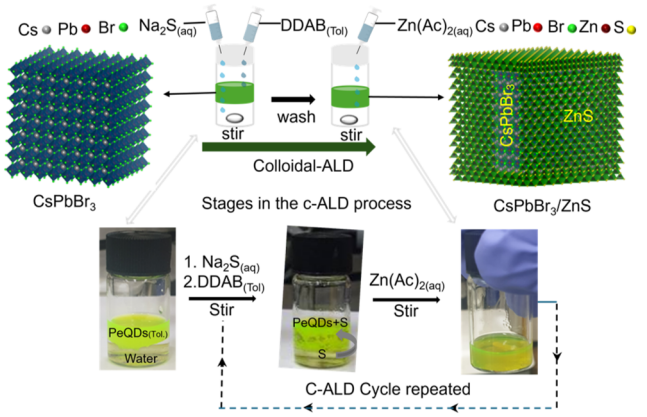

nm after one ZnS layer (1L, Figure S1b,e), and to 18.5 ± 1.5 nm after two ZnS layers(2L, Figures 1c and S1c,f), consistent with ZnS shell growth using the c-ALD method. After the ZnS shell growth via c-ALD, the size of the PeQDs increased, and a morphological change was observed.

High-resolution TEM images (Figure 1d) further confirm the formation of the core/shell structure, showing a well-defined cubic $CsPbBr_3$ core surrounded by a distinct ZnS shell. The estimated ZnS thickness as observed from the core through to the final two cycle c-ALD ranges from 0.9, 3.2, and 4.3 nm. The magnified High-resolution transmission electron microscopy (HRTEM) images (Figure 1e,1f) clearly show the interface between the core and the shell, with lattice fringes corresponding to the (200) planes of $CsPbBr_3$ with *d*-spacing of 0.29 nm (Figure S8a–c) and the (100) planes of ZnS with *d*-spacing of 0.33 nm from the inverse FFT (Figure S8d–f) providing direct evidence of the successful growth of the ZnS shell around the $CsPbBr_3$ core. Figure 2 shows an X-ray photoelectron spectroscopy (XPS) analysis that provides further evidence for the successful growth of the ZnS shell on the $CsPbBr_3$ core via the c-ALD process and reveals the chemical composition and interfacial interaction between the core and the shell. The XPS survey spectrum in Figure 2a confirms the presence of Cs, Pb, Br, S, and Zn elements in the $CsPbBr_3$/ZnS core/shell heterostructure. To confirm changes in the chemical composition induced by ZnS shell growth, we compared the high-resolution XPS spectra of the core/shell heterostructure with those of the pristine $CsPbBr_3$ PeQDs. Notably, as shown in Figure 2b–d, the binding energies of Cs 3d, Pb 4f, and Br 3d peaks shift toward higher values by 0.23, 0.31, and 0.29 eV, respectively, after the ZnS shelling, indicating strong electronic interactions between the core and shell. Additionally, the characteristic Zn 2p and S 2p peaks (Figure 2e–f), absent in the pristine $CsPbBr_3$ PeQDs, emerge after the c-ALD process, further confirming the successful formation of the ZnS shell. These results demonstrate the effective chemical coupling between the $CsPbBr_3$ core and the ZnS shell, facilitated by the c-ALD method.[47,57]

The c-ALD formation of the ZnS shell on the $CsPbBr_3$ core significantly enhances the optical properties of the resulting core/shell heterostructure. The ZnS shell is critical in enhancing the photoluminescence performance of the core/shell heterostructure; being a wide band gap material, it passivates the surface defects of the PeQDs and hence reduces the nonradiative decay pathway associated with the core.

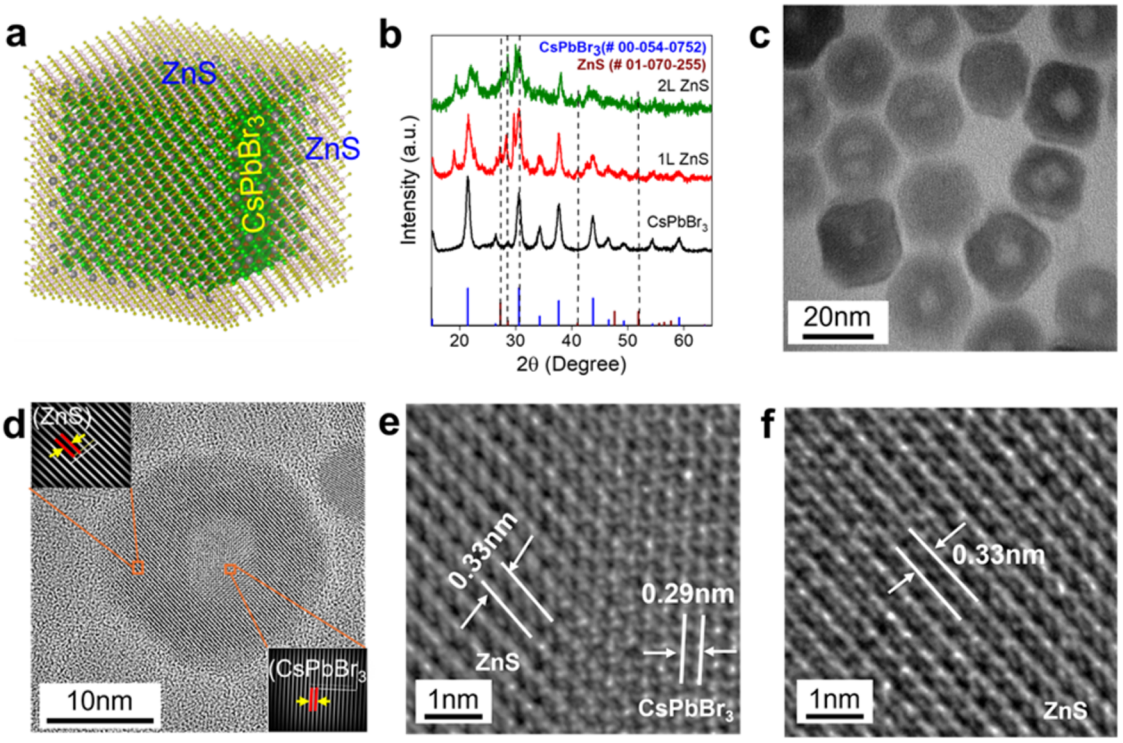

Figure 1. Structural characterization of $CsPbBr_3$/ZnS core/shell PeQDs. (a) Schematic illustration. (b) XRD patterns of pristine $CsPbBr_3$ and $CsPbBr_3$/ZnS. (c) HRTEM image of $CsPbBr_3$/ZnS. (d) HRTEM image showing clear lattice separation between the core and shell. (e) Enlarged image of core/shell interface. (f) Magnified lattice fringes of the ZnS shell.

https://doi.org/10.1021/jacsau.5c00651
JACS Au 2025, 5, 4036–4043

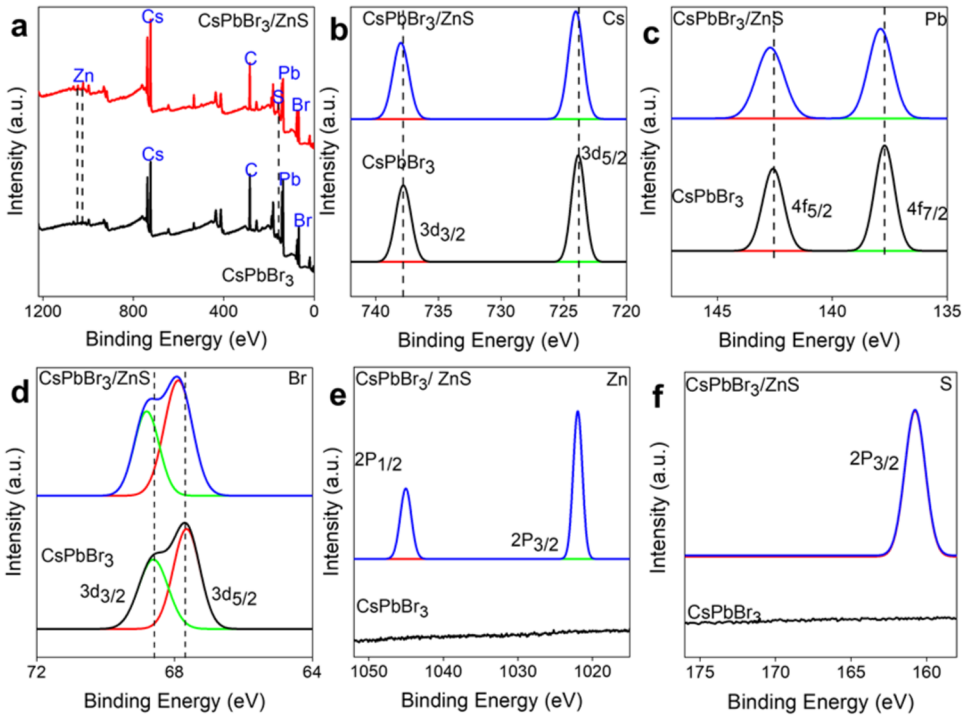

Figure 2. XPS analysis of pristine $CsPbBr_3$ and $CsPbBr_3$/ZnS core/shell PeQDs. (a) XPS survey spectra. (b–f) High-resolution XPS spectra of (b) Cs 3d, (c) Pb 4f, (d) Br 3d, (e) Zn 2p, and (f) S 2p.

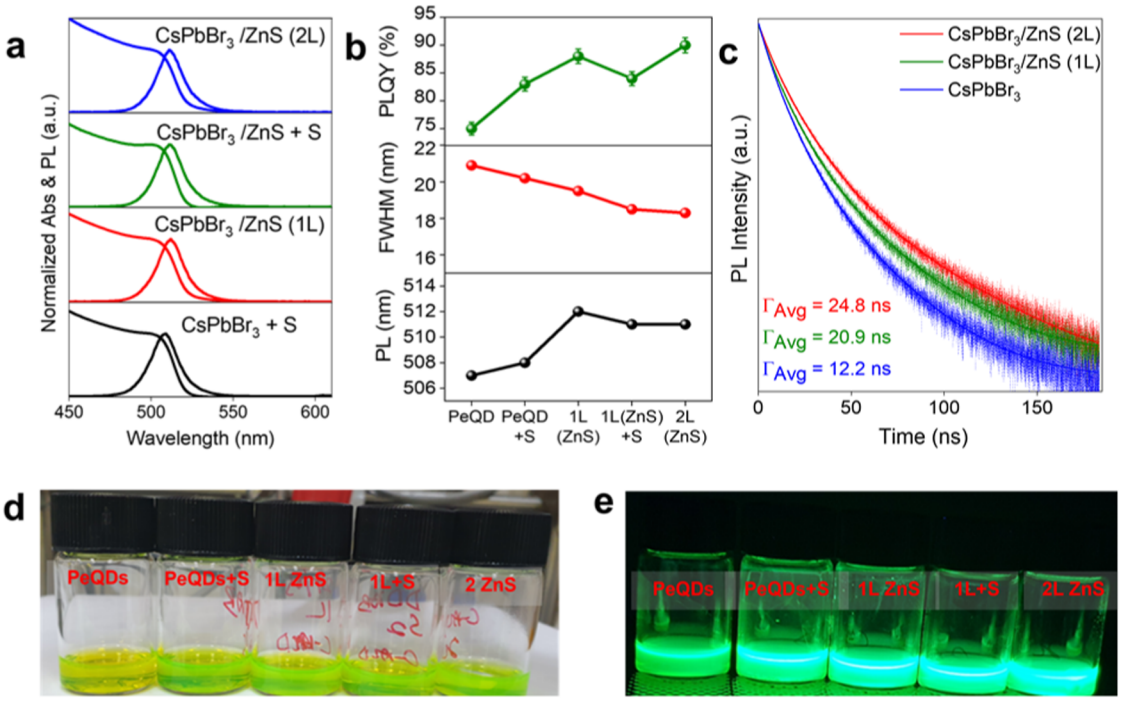

Figure 3. Optical properties of $CsPbBr_3$/ZnS core/shell PeQDs during c-ALD growth. (a) UV–vis absorption and PL spectra. (b) Optical parameter trends. (c) TRPL decay curves. (d, e) Photographic images under (d) room light and (e) UV light.

The absorption band-edge and photoluminescence (PL) spectra of the pristine $CsPbBr_3$ PeQDs are exhibited in Figure S2, while the evolution of these properties during the c-ALD shell cycle of the ZnS is shown in Figure 3a. Figure 3b summarizes the trends in key optical properties as a function of the c-ALD cycles. Notably, the PL peak position of $CsPbBr_3$ exhibits a redshift from 507 to 511 nm after two ZnS shell cycles, which is attributed to the partial diffusion of Zn or S ions into the $CsPbBr_3$ lattice and possible partial substitution of Pb ions.[46,50,58] This observation also suggests inorganic shell growth, a size increase (evidenced by TEM), and delocalization of excitonic wave functions across the core/shell interface over the core.[41,44,46,50] Furthermore, the PLQY of the pristine $CsPbBr_3$ PeQDs increases from 75 to 90% after two c-ALD

https://doi.org/10.1021/jacsau.5c00651
JACS Au 2025, 5, 4036–4043

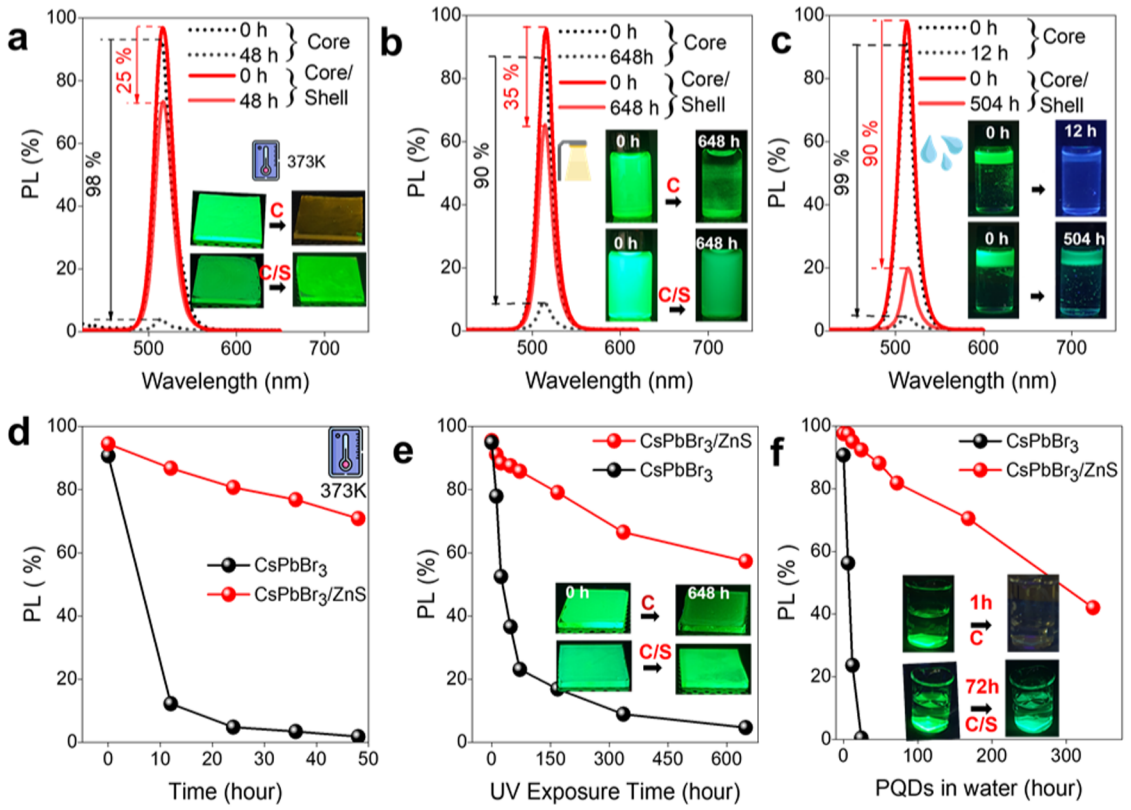

Figure 4. Stability comparison of pristine $CsPbBr_3$ and $CsPbBr_3$/ZnS core/shell PeQDs synthesized via c-ALD. (a) Thermal stability under heating at 373 K for 48 h. (b) Photostability under continuous UV irradiation. (c) Aqueous stability under water exposure. Insets in (a–c) show photographic images before and after each test. (d) Temperature-dependent PL at 373 K. (e) Relative PL intensity under UV irradiation. (f) Relative PL intensity in water under UV light. Insets in parts (e, f) show photographic images of corresponding thin films.

cycles, highlighting the effective passivation of surface defects by the ZnS shell. The 90% quantum yield of the $CsPbBr_3$/ZnS PeQDs synthesized via the c-ALD is comparable to the quantum yield value reported by the conventional one-pot and hot injection method.[20,50,57] However, an additional c-ALD cycle (third cycle) resulted in significant decreases in PL and other optical properties as shown in Figure S7. Figure 3d–e provides photographic images of $CsPbBr_3$ PeQDs at various c-ALD stages under ambient temperature and ultraviolet-lamp (UV-lamp) illumination, respectively. To investigate exciton recombination dynamics, time-resolved PL (TRPL) measurements were performed on pristine and $CsPbBr_3$/ZnS core/shell PeQDs using a 500 nm excitation source (Figure 3c). The decay profiles were fitted with a multiexponential function. The pristine $CsPbBr_3$ PeQDs exhibit a faster decay rate than the core/shell heterostructures, consistent with the PLQY enhancements.[47] The average PL lifetime increased from 12.2 ns (pristine) to 20.9 ns (one ZnS layer) and further to 24.8 ns (two ZnS layers), as summarized in Table S1. These results indicate that the ZnS shell effectively suppresses nonradiative recombination pathways, leading to prolonged exciton lifetimes and improved optical properties of the $CsPbBr_3$/ZnS core/shell heterostructure.[44,47]

To evaluate the impact of ZnS shell formation on the stability of $CsPbBr_3$ PeQDs, we systematically examined their thermal, photostability, and aqueous stability performances. The wide band gap of the ZnS shell provides a physical barrier to the PeQDs, which protects ion migration and enhances the environmental stability of the core/shell heterostructure. The results clearly demonstrate that the $CsPbBr_3$/ZnS core/shell heterostructure exhibits significantly enhanced resistance against external environmental stresses compared to pristine $CsPbBr_3$ PeQDs. As shown in Figure 4a, when subjected to heating at 373 K, the pristine $CsPbBr_3$ PeQDs rapidly lost nearly 98% of their initial PL intensity within 10 h, while the $CsPbBr_3$/ZnS core/shell heterostructure retained approximately 75% of its original emission intensity even after 50 h, exhibiting a much slower degradation profile. The inset of Figure 4a presents the photographic images of both samples before and after thermal exposure, visually highlighting the superior thermal durability of the core/shell structure.

In addition to thermal stability, the ZnS shell significantly enhances the photostability of the $CsPbBr_3$ PeQDs. As shown in Figure 4b, after 648 h of continuous UV irradiation, the pristine $CsPbBr_3$ PeQDs retained only ~10% of their initial PL intensity, whereas the $CsPbBr_3$/ZnS core/shell PeQDs maintained ~65% of their initial emission. The insets in Figure 4b,4e show photographic images of both samples under UV light, further confirming the enhanced photostability of the core/shell PeQDs. The pristine $CsPbBr_3$ PeQDs exhibited a steep decrease in the PL intensity over time (Figure S5a), while the core/shell heterostructure showed only a slight reduction (Figure S5b), as further demonstrated by the relative PL intensity plot in Figure 4e. It is worth emphasizing that this exceptional photostability can be directly correlated to the thicker ZnS shell formed by the c-ALD method. Previous reports have often suffered from rapid PL quenching due to incomplete surface coverage or thin shells prone to photo-induced degradation. In contrast, our thicker ZnS shell effectively blocks the penetration of oxygen, moisture, and

https://doi.org/10.1021/jacsau.5c00651
JACS Au 2025, 5, 4036–4043

photogenerated species, thereby preventing the structural and chemical degradation of the $CsPbBr_3$ core under prolonged light exposure. The aqueous stability of the PeQDs was also evaluated by monitoring PL intensity over time under continuous water exposure. Figure 4c,f reveals that the pristine $CsPbBr_3$ PeQDs suffered nearly complete degradation within 12 h, losing ~99% of their initial PL intensity. In stark contrast, the $CsPbBr_3$/ZnS core/shell heterostructure experienced only a 5% reduction in PL intensity during the first 12 h and retained approximately 10% of its initial intensity even after 504 h of water immersion. The photographic images of the samples before and after water exposure are shown in the inset of Figure 4c,4f for solution and thin film forms, respectively. These outstanding results clearly support the critical role of the thick ZnS shell in enhancing the long-term aqueous durability of the $CsPbBr_3$ PeQDs. The thick ZnS shell formed via the c-ALD significantly outperforms the previous reported ZnS shell using the conventional methods, which exhibits aqueous stability over 48−96 h.[44,47,57] While previous strategies employing thin oxide or sulfide shells have shown short-term water stability, the present work surpasses such reports by demonstrating continuous structural and optical integrity over an unprecedented time scale of more than 500 h of water exposure. Overall, the thick ZnS shell formed via the c-ALD process provides robust protection against thermal, photonic, and aqueous degradation, effectively enhancing the long-term stability of $CsPbBr_3$ PeQDs. Compared with previously reported core/shell $CsPbBr_3$ systems, our c-ALD-grown thick ZnS shell offers a clear advantage in terms of uniformity, scalability, and environmental resilience, representing a promising pathway for advancing durable perovskite nanomaterials for future optoelectronic applications.

CONCLUSIONS

We successfully demonstrated the room-temperature growth of a robust ZnS shell around $CsPbBr_3$ PeQDs via the colloidal-atomic layer deposition (c-ALD) process. The precise and uniform deposition enabled by c-ALD not only enhances the photophysical properties of $CsPbBr_3$ PeQDs, including a significant increase in PLQY and prolonged exciton lifetime, but also imparts exceptional stability against thermal stress, continuous UV irradiation, and long-term aqueous exposure. Notably, the formation of a relatively thicker and uniform ZnS shell, which is unattainable by conventional shelling methods, serves as a key factor in overcoming the inherent instability of $CsPbBr_3$ PeQDs. These findings highlight the versatility and potential of the c-ALD technique as a powerful strategy for engineering highly stable and efficient perovskite core/shell nanostructures, paving the way for their practical utilization in next-generation optoelectronic devices.

EXPERIMENTAL SECTION

Synthesis of $CsPbBr_3$ PeQDs

In a typical synthesis procedure, 0.764 mmol of $PbBr_2$, 2 mL of OA, and 20 mL of the ODE were loaded into a 50 mL three-neck flask. The mixture was vacuumed at 120 °C for 45 min. Then, 2 mL of 0.1 M DDAB in OLAM was injected and vacuumed, continuing to 60 min to remove air and moisture. The flask was purged with a N_2 gas flow, and the temperature was raised to 180 °C to dissolve the $PbBr_2$ completely. After the mixture stabilized, 2 mL of preheated as-prepared Cs-oleate was injected into the mixture, and after 5−10 s of QD's growth, the reaction was quenched with an ice bath to RT.[56,57] The crude solution was centrifuged at 8000 rpm for 10 min to remove the insoluble byproducts. The supernatant was discarded, and 10 mL of toluene was added to dissolve the precipitate. Finally, the $CsPbBr_3$ PQDs were purified using the precipitation/redispersion method with methyl acetate as an antisolvent.

Synthesis of ZnS Shell on $CsPbBr_3$ via c-ALD in Nonpolar Phase without Phase Transfer

In a 5 mL vial, 1 mL of aqua, 20 μL of 0.5 M Na_2S aqueous solution, 1 mL of purified $CsPbBr_3$ (30 mg/mL) in toluene, and 40 μL of DDAB were stirred at room temperature for 5 min. Combining toluene, DDAB solution, and aqua forms the liquid−liquid biphasic system, an essential parameter for the colloidal-atomic layer deposition. The $CsPbBr_3/S^{2-}$ form remains in the toluene phase stabilized by the DDA^- ligands, and the aqua phase was discarded. The nonpolar phase with $CsPbBr_3/S^2$ was washed with excess aqua to remove excess Sodium sulfide. Next, the biphasic system was reconstituted again by adding 1 mL of fresh aqua to $CsPbBr_3/S^{2-}$ solution, followed by the addition of a mixture of 10 μL of 0.5 M $Zn(Ac)_2$ in toluene-OLAM, and 10 μL $Zn(Ac)_{2(aq)}$, and stirred for 5 min. The aqua phase was discarded, and nonpolar hexane with PeQDs was washed to remove unreacted zinc acetate. By this process, the Zn^{2+} from the second stage of the c-ALD reacts with the S^{2-} surface from the first stage of the c-ALD process to form 1-layer ZnS on the $CsPbBr_3$ stabilized by the OLAM. The c-ALD cycle was repeated twice to grow two monolayers of ZnS layers on the $CsPbBr_3$. This process occurs without precipitation of the PeQDs after each monolayer growth.

ASSOCIATED CONTENT

Supporting Information

The Supporting Information is available free of charge at https://pubs.acs.org/doi/10.1021/jacsau.5c00651.

Additional experimental details, UV−visible absorption spectra, PL emission spectra, TEM, TRPL Fitting parameters, thermal, aqueous, and photostability PL data (PDF)

AUTHOR INFORMATION

Corresponding Author

Jong-Soo Lee − *Department of Energy Science & Engineering, Daegu Gyeongbuk Institute of Science and Technology (DGIST), Daegu 42988, Republic of Korea;* orcid.org/0000-0002-3045-2206; Email: jslee@dgist.ac.kr

Authors

Justice A. Teku − *Department of Energy Science & Engineering, Daegu Gyeongbuk Institute of Science and Technology (DGIST), Daegu 42988, Republic of Korea*

Derrick A. Taylor − *Department of Energy Science & Engineering, Daegu Gyeongbuk Institute of Science and Technology (DGIST), Daegu 42988, Republic of Korea*

Complete contact information is available at: https://pubs.acs.org/10.1021/jacsau.5c00651

Notes

The authors declare no competing financial interest.

ACKNOWLEDGMENTS

J.-S. Lee acknowledges the financial support from the National Research Council of Science & Technology (NST) grant (No. CAP 23071-300) funded by the Korea government (MSIT).

REFERENCES

(1) Protesescu, L.; Yakunin, S.; Bodnarchuk, M. I.; Krieg, F.; Caputo, R.; Hendon, C. H.; Yang, R. X.; Walsh, A.; Kovalenko, M. V.

Nanocrystals of Cesium Lead Halide Perovskites (CsPbX(3), X = Cl, Br, and I): Novel Optoelectronic Materials Showing Bright Emission with Wide Color Gamut. *Nano Lett.* **2015**, *15* (6), 3692−3696.
(2) Nedelcu, G.; Protesescu, L.; Yakunin, S.; Bodnarchuk, M. I.; Grotevent, M. J.; Kovalenko, M. V. Fast Anion-Exchange in Highly Luminescent Nanocrystals of Cesium Lead Halide Perovskites (CsPbX3, X = Cl, Br, I). *Nano Lett.* **2015**, *15* (8), 5635−5640.
(3) Di Stasio, F.; Christodoulou, S.; Huo, N.; Konstantatos, G. Near-Unity Photoluminescence Quantum Yield in CsPbBr3 Nanocrystal Solid-State Films via Postsynthesis Treatment with Lead Bromide. *Chem. Mater.* **2017**, *29* (18), 7663−7667.
(4) Koscher, B. A.; Swabeck, J. K.; Bronstein, N. D.; Alivisatos, A. P. Essentially Trap-Free CsPbBr(3) Colloidal Nanocrystals by Post-synthetic Thiocyanate Surface Treatment. *J. Am. Chem. Soc.* **2017**, *139* (19), 6566−6569.
(5) Liu, F.; Zhang, Y.; Ding, C.; Kobayashi, S.; Izuishi, T.; Nakazawa, N.; Toyoda, T.; Ohta, T.; Hayase, S.; Minemoto, T.; Yoshino, K.; Dai, S.; Shen, Q. Highly Luminescent Phase-Stable CsPbI(3) Perovskite Quantum Dots Achieving Near 100% Absolute Photoluminescence Quantum Yield. *ACS Nano* **2017**, *11* (10), 10373−10383.
(6) Jena, A. K.; Kulkarni, A.; Miyasaka, T. Halide Perovskite Photovoltaics: Background, Status, and Future Prospects. *Chem. Rev.* **2019**, *119* (5), 3036−3103.
(7) Swarnkar, A.; Marshall, A. R.; Sanehira, E. M.; Chernomordik, B. D.; Moore, D. T.; Christians, J. A.; Chakrabarti, T.; Luther, J. M. Quantum dot−induced phase stabilization of α-CsPbI3 perovskite for high-efficiency photovoltaics. *Science* **2016**, *354* (6308), 92−95.
(8) Dey, A.; Ye, J.; De, A.; Debroye, E.; Ha, S. K.; Bladt, E.; Kshirsagar, A. S.; Wang, Z.; Yin, J.; Wang, Y.; Quan, L. N.; Yan, F.; Gao, M.; Li, X.; Shamsi, J.; Debnath, T.; Cao, M.; Scheel, M. A.; Kumar, S.; Steele, J. A.; Gerhard, M.; Chouhan, L.; Xu, K.; Wu, X. G.; Li, Y.; Zhang, Y.; Dutta, A.; Han, C.; Vincon, I.; Rogach, A. L.; Nag, A.; Samanta, A.; Korgel, B. A.; Shih, C. J.; Gamelin, D. R.; Son, D. H.; Zeng, H.; Zhong, H.; Sun, H.; Demir, H. V.; Scheblykin, I. G.; Mora-Sero, I.; Stolarczyk, J. K.; Zhang, J. Z.; Feldmann, J.; Hofkens, J.; Luther, J. M.; Perez-Prieto, J.; Li, L.; Manna, L.; Bodnarchuk, M. I.; Kovalenko, M. V.; Roeffaers, M. B. J.; Pradhan, N.; Mohammed, O. F.; Bakr, O. M.; Yang, P.; Muller-Buschbaum, P.; Kamat, P. V.; Bao, Q.; Zhang, Q.; Krahne, R.; Galian, R. E.; Stranks, S. D.; Bals, S.; Biju, V.; Tisdale, W. A.; Yan, Y.; Hoye, R. L. Z.; Polavarapu, L. State of the Art and Prospects for Halide Perovskite Nanocrystals. *ACS Nano* **2021**, *15* (7), 10775−10981.
(9) Li, J.; Xu, L.; Wang, T.; Song, J.; Chen, J.; Xue, J.; Dong, Y.; Cai, B.; Shan, Q.; Han, B.; Zeng, H. 50-Fold EQE Improvement up to 6.27% of Solution-Processed All-Inorganic Perovskite CsPbBr3 QLEDs via Surface Ligand Density Control. *Adv. Mater.* **2017**, *29* (5), No. 1603885.
(10) Zhang, X.; Xu, B.; Zhang, J.; Gao, Y.; Zheng, Y.; Wang, K.; Sun, X. W. All-Inorganic Perovskite Nanocrystals for High-Efficiency Light Emitting Diodes: Dual-Phase CsPbBr3-CsPb2Br5 Composites. *Adv. Funct. Mater.* **2016**, *26* (25), 4595−4600.
(11) Hassan, Y.; Park, J. H.; Crawford, M. L.; Sadhanala, A.; Lee, J.; Sadighian, J. C.; Mosconi, E.; Shivanna, R.; Radicchi, E.; Jeong, M.; Yang, C.; Choi, H.; Park, S. H.; Song, M. H.; De Angelis, F.; Wong, C. Y.; Friend, R. H.; Lee, B. R.; Snaith, H. J. Ligand-engineered bandgap stability in mixed-halide perovskite LEDs. *Nature* **2021**, *591* (7848), 72−77.
(12) Manser, J. S.; Christians, J. A.; Kamat, P. V. Intriguing Optoelectronic Properties of Metal Halide Perovskites. *Chem. Rev.* **2016**, *116* (21), 12956−13008.
(13) Quan, L. N.; Rand, B. P.; Friend, R. H.; Mhaisalkar, S. G.; Lee, T. W.; Sargent, E. H. Perovskites for Next-Generation Optical Sources. *Chem. Rev.* **2019**, *119* (12), 7444−7477.
(14) Pacchioni, G. Highly efficient perovskite LEDs. *Nat. Rev. Mater.* **2021**, *6* (2), 108.
(15) Veldhuis, S. A.; Boix, P. P.; Yantara, N.; Li, M.; Sum, T. C.; Mathews, N.; Mhaisalkar, S. G. Perovskite Materials for Light-Emitting Diodes and Lasers. *Adv. Mater.* **2016**, *28* (32), 6804−6834.
(16) Zhu, H.; Fu, Y.; Meng, F.; Wu, X.; Gong, Z.; Ding, Q.; Gustafsson, M. V.; Trinh, M. T.; Jin, S.; Zhu, X. Y. Lead halide perovskite nanowire lasers with low lasing thresholds and high quality factors. *Nat. Mater.* **2015**, *14* (6), 636−642.
(17) Dong, Y.; Gu, Y.; Zou, Y.; Song, J.; Xu, L.; Li, J.; Xue, J.; Li, X.; Zeng, H. Improving All-Inorganic Perovskite Photodetectors by Preferred Orientation and Plasmonic Effect. *Small* **2016**, *12* (40), 5622−5632.
(18) Tian, W.; Zhou, H.; Li, L. Hybrid Organic−Inorganic Perovskite Photodetectors. *Small* **2017**, *13* (41), No. 1702107.
(19) Gong, M.; Sakidja, R.; Goul, R.; Ewing, D.; Casper, M.; Stramel, A.; Elliot, A.; Wu, J. Z. High-Performance All-Inorganic CsPbCl3 Perovskite Nanocrystal Photodetectors with Superior Stability. *ACS Nano* **2019**, *13* (2), 1772−1783.
(20) Chen, K.; Liu, D.; Lu, W.; Zhuo, K.; Li, G. Surface and Interface Engineering for Highly Stable CsPbBr3/ZnS Core/Shell Nanocrystals. *Inorg. Chem.* **2024**, *63* (4), 2247−2256.
(21) Ye, C.; Jiang, J.; Zou, S.; Mi, W.; Xiao, Y. Core−Shell Three-Dimensional Perovskite Nanocrystals with Chiral-Induced Spin Selectivity for Room-Temperature Spin Light-Emitting Diodes. *J. Am. Chem. Soc.* **2022**, *144* (22), 9707−9714.
(22) Tang, X.; Yang, J.; Li, S.; Liu, Z.; Hu, Z.; Hao, J.; Du, J.; Leng, Y.; Qin, H.; Lin, X.; Lin, Y.; Tian, Y.; Zhou, M.; Xiong, Q. Single Halide Perovskite/Semiconductor Core/Shell Quantum Dots with Ultrastability and Nonblinking Properties. *Adv. Sci.* **2019**, *6* (18), No. 1900412.
(23) Chen, K.; Wang, C.; Peng, Z.; Qi, K.; Guo, Z.; Zhang, Y.; Zhang, H. The chemistry of colloidal semiconductor nanocrystals: From metal-chalcogenides to emerging perovskite. *Coord. Chem. Rev.* **2020**, *418*, No. 213333.
(24) Zhang, X.; Yin, W.; Zheng, W.; Rogach, A. L. Perovskite Quantum Dots with Atomic Crystal Shells for Light-Emitting Diodes with Low Efficiency Roll-Off. *ACS Energy Lett.* **2020**, *5* (9), 2927−2934.
(25) Bera, S.; Pradhan, N. Perovskite Nanocrystal Heterostructures: Synthesis, Optical Properties, and Applications. *ACS Energy Lett.* **2020**, *5* (9), 2858−2872.
(26) Ahmed, G. H.; Yin, J.; Bakr, O. M.; Mohammed, O. F. Successes and Challenges of Core/Shell Lead Halide Perovskite Nanocrystals. *ACS Energy Lett.* **2021**, *6* (4), 1340−1357.
(27) Akkerman, Q. A.; Raino, G.; Kovalenko, M. V.; Manna, L. Genesis, challenges and opportunities for colloidal lead halide perovskite nanocrystals. *Nat. Mater.* **2018**, *17* (5), 394−405.
(28) An, M. N.; Park, S.; Brescia, R.; Lutfullin, M.; Sinatra, L.; Bakr, O. M.; De Trizio, L.; Manna, L. Low-Temperature Molten Salts Synthesis: CsPbBr3 Nanocrystals with High Photoluminescence Emission Buried in Mesoporous SiO2. *ACS Energy Lett.* **2021**, *6* (3), 900−907.
(29) Zhong, Q.; Cao, M.; Hu, H.; Yang, D.; Chen, M.; Li, P.; Wu, L.; Zhang, Q. One-Pot Synthesis of Highly Stable CsPbBr(3)@SiO(2) Core-Shell Nanoparticles. *ACS Nano* **2018**, *12* (8), 8579−8587.
(30) Liu, H.; Tan, Y.; Cao, M.; Hu, H.; Wu, L.; Yu, X.; Wang, L.; Sun, B.; Zhang, Q. Fabricating CsPbX3-Based Type I and Type II Heterostructures by Tuning the Halide Composition of Janus CsPbX3/ZrO2 Nanocrystals. *ACS Nano* **2019**, *13* (5), 5366−5374.
(31) Li, Z.-J.; Hofman, E.; Li, J.; Davis, A. H.; Tung, C.-H.; Wu, L.-Z.; Zheng, W. Photoelectrochemically Active and Environmentally Stable CsPbBr3/TiO2 Core/Shell Nanocrystals. *Adv. Funct. Mater.* **2018**, *28* (1), No. 1704288.
(32) Loiudice, A.; Saris, S.; Oveisi, E.; Alexander, D. T. L.; Buonsanti, R. CsPbBr3 QD/AlO Inorganic Nanocomposites with Exceptional Stability in Water, Light, and Heat. *Angew. Chem., Int. Ed.* **2017**, *56* (36), 10696−10701.
(33) Lapointe, V.; Green, P. B.; Chen, A. N.; Buonsanti, R.; Majewski, M. B. Long live(d) CsPbBr3 superlattices: colloidal atomic layer deposition for structural stability. *Chem. Sci.* **2024**, *15* (12), 4510−4518.

https://doi.org/10.1021/jacsau.5c00651
JACS Au 2025, 5, 4036−4043

(34) Green, P. B.; Lecina, O. S.; Albertini, P. P.; Loiudice, A.; Buonsanti, R. Colloidal-ALD-Grown Metal Oxide Shells Enable the Synthesis of Photoactive Ligand/Nanocrystal Composite Materials. *J. Am. Chem. Soc.* **2023**, *145* (14), 8189−8197.
(35) Wang, B.; Zhang, C.; Huang, S.; Li, Z.; Kong, L.; Jin, L.; Wang, J.; Wu, K.; Li, L. Postsynthesis Phase Transformation for CsPbBr3/Rb4PbBr6 Core/Shell Nanocrystals with Exceptional Photostability. *ACS Appl. Mater. Interfaces* **2018**, *10* (27), 23303−23310.
(36) Wang, S.; Bi, C.; Yuan, J.; Zhang, L.; Tian, J. Original Core−Shell Structure of Cubic CsPbBr3@Amorphous CsPbBrx Perovskite Quantum Dots with a High Blue Photoluminescence Quantum Yield of over 80%. *ACS Energy Lett.* **2018**, *3* (1), 245−251.
(37) Zhu, B. S.; Li, H. Z.; Ge, J.; Li, H. D.; Yin, Y. C.; Wang, K. H.; Chen, C.; Yao, J. S.; Zhang, Q.; Yao, H. B. Room temperature precipitated dual phase CsPbBr(3)-CsPb(2)Br(5) nanocrystals for stable perovskite light emitting diodes. *Nanoscale* **2018**, *10* (41), 19262−19271.
(38) Qiu, H.; Li, F.; He, S.; Shi, R.; Han, Y.; Abudukeremu, H.; Zhang, L.; Zhang, Y.; Wang, S.; Liu, W.; Ma, C.; Fang, H.; Long, R.; Wu, K.; Zhang, H.; Li, J. Epitaxial CsPbBr(3) /CdS Janus Nanocrystal Heterostructures for Efficient Charge Separation. *Adv. Sci.* **2023**, *10* (13), No. 2206560.
(39) Tang, X.; Yang, J.; Li, S.; Chen, W.; Hu, Z.; Qiu, J. CsPbBr(3)/CdS Core/Shell Structure Quantum Dots for Inverted Light-Emitting Diodes Application. *Front. Chem.* **2019**, *7*, No. 499.
(40) Kipkorir, A.; DuBose, J.; Cho, J.; Kamat, P. V. CsPbBr(3)-CdS heterostructure: stabilizing perovskite nanocrystals for photocatalysis. *Chem. Sci.* **2021**, *12* (44), 14815−14825.
(41) Shi, J.; Ge, W.; Zhu, J.; Saruyama, M.; Teranishi, T. Core−Shell CsPbBr3@CdS Quantum Dots with Enhanced Stability and Photoluminescence Quantum Yields for Optoelectronic Devices. *ACS Appl. Nano Mater.* **2020**, *3* (8), 7563−7571.
(42) Gao, L.; Zeng, K.; Jia, Y.; Kong, L.; Liu, A.; Ma, T.; Bao, J. A Strain-Free Semicoherent Interface Achieved via Epitaxial Growth of CsPbBr3 on CdS Quantum Dots. *Cryst. Growth Des.* **2024**, *24* (9), 3581−3588.
(43) Vighnesh, K.; Sergeev, A. A.; Hassan, M. S.; Portniagin, A. S.; Sokolova, A. V.; Zhu, D.; Sergeeva, K. A.; Kershaw, S. V.; Wong, K. S.; Rogach, A. L. Red-Emitting CsPbI3/ZnSe Colloidal Nanoheterostructures with Enhanced Optical Properties and Stability. *Small* **2024**, *20* (40), No. 2400745.
(44) Ravi, V. K.; Saikia, S.; Yadav, S.; Nawale, V. V.; Nag, A. CsPbBr3/ZnS Core/Shell Type Nanocrystals for Enhancing Luminescence Lifetime and Water Stability. *ACS Energy Lett.* **2020**, *5* (6), 1794−1796.
(45) Chen, W.; Hao, J.; Hu, W.; Zang, Z.; Tang, X.; Fang, L.; Niu, T.; Zhou, M. Enhanced Stability and Tunable Photoluminescence in Perovskite CsPbX(3) /ZnS Quantum Dot Heterostructure. *Small* **2017**, *13* (21), No. 1604085.
(46) Liu, X.; Zhang, X.; Yu, S.; Li, L.; Xu, J.; Gong, X.; Ding, R.; Zhang, J.; Yin, H. Epitaxial growth of highly stable perovskite CsPbBr(3)/nZnS/Al core/multi-shell quantum dots with aluminium self-passivation. *Nanotechnology* **2020**, *31* (37), No. 375703.
(47) Hong, Y.; Yu, C.; Je, H.; Park, J. Y.; Kim, T.; Baik, H.; Tomboc, G. M.; Kim, Y.; Ha, J. M.; Joo, J.; Kim, C. W.; Woo, H. Y.; Park, S.; Choi, D. H.; Lee, K. Perovskite Nanocrystals Protected by Hermetically Sealing for Highly Bright and Stable Deep-Blue Light-Emitting Diodes. *Adv. Sci.* **2023**, *10* (23), No. 2302906.
(48) Zhou, H.; Wang, S.; Wang, H.; Wang, L.; Chen, J.; Jia, G.; Yang, X. CsZnPbBr3/ZnS core/shell perovskite nanocrystals for stable and efficient white light-emitting diodes. *Nanoscale* **2024**, *16* (20), 10064−10070.
(49) Livakas, N.; Zito, J.; Ivanov, Y. P.; Otero-Martínez, C.; Divitini, G.; Infante, I.; Manna, L. Nanocrystal Heterostructures Based on Halide Perovskites and Metal Sulfides. *J. Am. Chem. Soc.* **2024**, *146* (40), 27571−27582.
(50) Wang, P.; Wu, Z.; Wu, M.; Wei, J.; Sun, Y.; Zhao, Z. All-solution-processed, highly efficient and stable green light-emitting devices based on Zn-doped CsPbBr3/ZnS heterojunction quantum dots. *J. Mater. Sci.* **2021**, *56* (6), 4161−4171.
(51) Nasilowski, M.; Nienhaus, L.; Bertram, S. N.; Bawendi, M. G. Colloidal atomic layer deposition growth of PbS/CdS core/shell quantum dots. *Chem. Commun.* **2017**, *53* (5), 869−872.
(52) Ithurria, S.; Talapin, D. V. Colloidal Atomic Layer Deposition (c-ALD) using Self-Limiting Reactions at Nanocrystal Surface Coupled to Phase Transfer between Polar and Nonpolar Media. *J. Am. Chem. Soc.* **2012**, *134* (45), 18585−18590.
(53) Loiudice, A.; Saris, S.; Oveisi, E.; Alexander, D. T. L.; Buonsanti, R. CsPbBr(3) QD/AlO(x) Inorganic Nanocomposites with Exceptional Stability in Water, Light, and Heat. *Angew. Chem., Int. Ed.* **2017**, *56* (36), 10696−10701.
(54) Loiudice, A.; Lecina, O. S.; Bornet, A.; Luther, J. M.; Buonsanti, R. Ligand Locking on Quantum Dot Surfaces via a Mild Reactive Surface Treatment. *J. Am. Chem. Soc.* **2021**, *143* (33), 13418−13427.
(55) Loiudice, A.; Strach, M.; Saris, S.; Chernyshov, D.; Buonsanti, R. Universal Oxide Shell Growth Enables in Situ Structural Studies of Perovskite Nanocrystals during the Anion Exchange Reaction. *J. Am. Chem. Soc.* **2019**, *141* (20), 8254−8263.
(56) Wu, H.; Zhang, Y.; Lu, M.; Zhang, X.; Sun, C.; Zhang, T.; Colvin, V. L.; Yu, W. W. Surface ligand modification of cesium lead bromide nanocrystals for improved light-emitting performance. *Nanoscale* **2018**, *10* (9), 4173−4178.
(57) Teku, J. A.; Lee, N.; Taylor, D. A.; Selvaraj, J.; Lee, J.-S. Highly Stable CsPbBr3 Perovskite Quantum Dots with ZnS Shells from Single-Molecule Precursors for Optoelectronic Devices. *ACS Appl. Nano Mater.* **2024**, *7* (17), 20034−20045.
(58) van der Stam, W.; Geuchies, J. J.; Altantzis, T.; van den Bos, K. H. W.; Meeldijk, J. D.; Van Aert, S.; Bals, S.; Vanmaekelbergh, D.; de Mello Donega, C. Highly Emissive Divalent-Ion-Doped Colloidal CsPb1−xMxBr3 Perovskite Nanocrystals through Cation Exchange. *J. Am. Chem. Soc.* **2017**, *139* (11), 4087−4097.

https://doi.org/10.1021/jacsau.5c00651
JACS Au 2025, 5, 4036−4043